RSC Advances

Journal Name

ARTICLE

Zeolite encapsulated active metal composites and their photocatalytic studies for the rhodamine-b, reactive red-198 and chloro- phenols

G. Ramanjaneya Reddy[a], S. Balasubramanian[a], K. Chennakesavulu[b,c*]

Niobium (Nb), tantalum (Ta) and palladium (Pd) were impregnated in the cavities of zeolite by the ion exchange method. The impregnation and composites stability were investigated by FTIR, DRS/UV-Visible, XRD, XPS, BET, N_2 adsorption isotherms, AAS, FESEM/EDX, TEM, TGA and particle size. The composites denoted as PdY, NbPdY and TaPdY were used as visible light driven photocatalysts in the degradation of Rhodamine-B (RhB), Reactive red-198 (RR), 2-chloro phenol (2CP) and 4-chloro phenol (4CP) under visible light irradiation. The composites catalytic ability was determined by the UV-visible absorption spectral analysis. The TaPdY, NbPdY were exhibits superior degradation kinetics when compared to that of PdY and NaY, due to presence of refractory metals such as Nb(V) and Ta(V) in the zeolite cavities. The percentage of degradation and rate of reaction is more for NbPdY and TaPdY. The photo oxidation reaction follows the *pseudo*-first order reaction kinetics and it might be due to the fixed concentration of the reactants, photocatalysts and reaction medium. The NbPdY and TaPdY catalysts are recoverable and reusable upto five cycles of repeated usage. Thus, a recovered and reusable catalyst shows comparable activity with fresh catalyst.

Introduction

Transition metal oxides and metal complexes were widely used in the field of catalysis and photocatalysis.[1-3] The Nb and Ta oxides are potential materials in the heterogeneous catalysis reactions for organic transformations,[4-6] due to their inert nature, eco-friendly, biocompatible and thermally stable. This can act as surface active catalysts with help porous materials such as zeolite, MCM41 and SBA15.[7,8] In recent years, usage of the nanocomposite has been widely documented in the photocatalysis, waste water treatment, fuel cells, energy sectors, gas storage, sensors, bio-imaging, medicine, optics, non-corrosive and drug delivery systems etc.[9,10]

The NaY zeolite has been receive growing interest in the degradation of a variety of synthetic toxic organic compounds.[11-14] The transition metal ions such as Ni, Cu, Zn, Ru, Nb, Ta and Pd can be impregnated in the cavities of NaY, they could act as good catalysts.[15,16] The great attention requires to treat the water contaminations by the semiconducting metals and zeolites. The UV/Visible light responded degradation of organic dyes eluted

from the textile, food, chemical industries are a challenging task. The food and agriculture organization and world health organization (WHO) also evaluated importance of the composite materials to environmental pollution.[17] The major global problem is to increase food production with limited resources and minimize usage of the fertilizer and pesticides without polluting the environment. Synthetic dyes are excellent light harvesting materials, but they are considered as environmental hazards, when its discharges into water bodies. Some of the cationic, anionic dyes and halo-phenolic derivatives are cause water contamination. The methyl orange, RhB, phenol red, xylenol orange, chlorophenol etc, were few examples for common organic pollutants, which are released from the textile, food and agricultural industries. During the treatment of waste water in municipals, chlorophenols are formed as an active intermediates.[18,19]

The mineralization of toxic pollutants to less toxic products like carbon dioxide, water, and inorganic mineral ions under solar light source by NaY composites could be used effectively. The degradation ability of NbPdY and TaPdY composites depends on the electron-hole recombination at the surface of catalyst and dye can decrease the excitation of an electron (e^-) from the valence band (VB) to conduction band (CB) of the photocatalyst, leaving a photogenerated hole (h^+). This creates hydroxyl and peroxy ions in aqueous solution thus facilitating catalytic activities.[20,21] Nascent oxygen also play a key role in the process of degradation and the $^{\bullet}$OH radial-ions also performed well in the degradation of mechanisms.[22] Hence, synthetic importance of the porous composites with refractory metals and importance in the degradation of toxic cationic, anionic, and halo-phenols under UV and solar light source has been raised.[23] A comprehensive examination of the published literature does reveal the synthesis of solid supported Nb

a. *Department of Inorganic Chemistry, Guindy Campus, University of Madras, Chennai - 600 025, India.Email.gonturamunom@gmail.com*
b. *Department of Chemistry, Sathyabama University, Chennai-600 119, India. Tel/Fax:+914424503814.*
c. *Centre for Nano Science and Nano Technolgy, International Research Centre, Sathyabama University, Chennai-600 119. Email: chennanml@yahoo.com.*

and Ta composites and their usages in photocatalysis applications yet to be reported.

In the present investigation an attempt was made to synthesis of Pd(II) exchanged NaY porous moiety and then subsequently impregnated by Nb and Ta chloride salts. The porous composites were used as photocatalyst in the degradation of RhB, RR, 2-CP and 4-CP under visible light irradiation. Spectrophotometric techniques have been employed for the determination of degradation ability of the composite materials. The reused solid catalyst, catalytic performance was compared with the fresh catalyst.

Experimental

Materials

Palladium chloride, Niobium chloride, Tantalum chloride, Zeolite-Y (Si/Al=2.7, $Na_{52}[(AlO_2)_{52}(SiO_2)_{140}]$), Rhodamine-B (Sigma-Aldrich, India), Reactive red-198 (Textile industry, Tamilnadu), 2-chlorophenol, 4-chlorophenol (Merck Pvt. Ltd, India) were used without further purification. Millipore water was used throughout the work.

Physicochemical measurements and characterization

The FTIR spectra were recorded on a FTIR Perkin-Elmer 8300 spectrometer with KBr disk. The UV-visible Diffuse Reflectance Spectral (UV-Visible/DRS) analyses were carried out on a JASCO-V-670 UV-Visible spectrophotometer. The XPS analysis was carried out on Kratos AXIS 165 XPS system with Mg-Kα monochromatic wavelength. All the samples were made in to pellets and were used as such for X-ray Photoelectron Spectroscopic (XPS) studies. The high resolution XPS traces were deconvoluted using the Gaussian statistical analysis by using origin-7 software. The crystalline nature of the NaY, PdY, NbPdY and TaPdY was ascertained by the powder X-ray diffraction using Rigaku XRD-Smart Lab with Cu-Kα₁ radiation (λ=1.5418 Aº). TGA experiments were performed with Versa Therm Cahn Thermo balance TG-151 with a sensitivity of 10μg. TGA experiments were conducted in the temperature range of 300-1200 K with 50 ± 0.01 mg of the samples and the analyses were carried out at a heating rate of 10 K/ min under static air atmosphere. The Brunauer-Emmett-Teller (BET) surface area and N_2 adsorption-desorption isotherms were obtained using a Micrometrics ASAP (Model 2020) surface area analyzer with nitrogen and helium gases with a purity of 99.999%. The scanning electron micrograph (SEM) was obtained on a FESEM-SUPRA 55- CARL ZEISS scanning electron microscope. HRTEM analysis was carried out by using a FEI TECNAI G2 (T-30) transmission electron microscope with an accelerating voltage of 250 KV. The particle size distribution curves of all composites were obtained in the aqueous medium by using the CILAS 1180.

Synthesis of the PdY

The Palladium chloride (3.54 mg) was added to the 50 mL of acidic aqueous solution with 1 g of NaY and mixture was stirred for 8 h at 368 K. The obtained grey color solid were filtered, washed with 50 mL of hot distilled water and dried under vacuum for 5 h at 363 K.

Synthesis of the PdNbY

0.5 g of the PdY was well suspended in ethanol and toluene mixture and then the 2.7 mg of Nb chloride was added in under nitrogen atm and continue heating at 363 K for 12 h. The resulting light grey color solid was washed with 0.1M NaCl aqueous solution and filtered, the resulting solid Soxhlet extracted with the ethanol for 4 h and acetone for 3 h. The final light grey color solid was dried at 423 K for 3 h.

Synthesis of the PdTaY

0.5 g of the PdY was well suspended in toluene and ethanol mixture, 3.6 mg of Ta chloride was added to it under nitrogen atm, continue heating at 363 K for 12 h. The resulting grey solid was washed with 0.1M NaCl aqueous solution and filtered then the resulting solid soxhlet extracted with the ethanol 4 h and acetone for 3 h. The final light grey color solid was dried at 423 K for 3 h solid was heated at 423 K for 3 h.

Photocatalytic degradation of the RhB under visible light irradiation

The photocatalytic activities of the NaY, PdY, NbPdY and TaPdY in degradation of the RhB under visible light in a cylindrical glass reactor with a diameter of 75 × 100mm that contains a water jacket at room temperature. A 250 W tungsten lamp (Philips) used as a visible light source equipped with a UV cut-off filter was used to carried out photoxidation reactions. The glass reactor with the catalyst 0.05 g of NaY / 0.05 g of PdY / 0.05 g of NbPdY and 0.05 g of TaPdY and 0.01 mmol of 100 mL aqueous dye solution was added. The reaction conditions are optimized in dark at room temperature and start irradiation under visible light. The RhB dye removal percentage and consequent spectral changes at predetermined time intervals were monitored by the UV-visible absorption spectra, at 554±1 nm for 2.5 h. The percentage conversion is calculated from equation (1).

$$A = \varepsilon.c.l \qquad (1)$$

Here ε = molar extinction coefficient [M⁻¹ cm⁻¹], c = sample concentration and l = path length of cuvette (1 cm).

Photocatalytic degradation of the RR under visible light irradiation

The photocatalytic activities of the NaY, PdY, NbPdY and TaPdY in degradation of the RR under visible light in a cylindrical glass reactor with the glass reactor with the catalyst 0.05 g of NaY /0.05 g PdY/ 0.05 g of NbPdY and 0.05 g of TaPdY and 0.01 mmol of 100 mL aqueous dye solution was added to the catalysts separately. The reaction conditions are optimized in dark at room temperature and start irradiation under visible light. The dye removal percentage and consequent spectral changes at predetermined time intervals were monitored by the UV-visible absorption spectra, at 519±1 nm for 5.5 h. The percentage conversion is calculated from equation (1).

ARTICLE

Degradation of 2-chlorophenol in the presence of NaY, PdY, NbPdY and TaPdY

The absorption spectrum of 2-CP exhibits λ_{max} values at 216 nm and 276 nm. No detectable absorption is present above 310 nm. The reaction conditions are optimized in dark at room temperature and start irradiation under visible light (> 380 nm). The removal percentage and consequent spectral changes at predetermined time intervals were monitored by the UV-visible absorption spectra at 276 ± 1 nm for 4.5 h. The percentage conversion was calculated from equation (1).

Degradation of 4-chlorophenol in the NaY, PdY, NbPdY and TaPdY

The 4-CP absorption spectrum exhibits λ_{max} values at 220 nm and 280 nm. No detectable absorption is present above 310 nm. The reaction conditions are optimized in dark at room temperature and start irradiation under visible light (>380 nm). The removal percentage and consequent spectral changes at predetermined time intervals were monitored by the UV-visible absorption spectra at 220 ± 1 nm for 3 h. The percentage conversion is calculated from equation (1).

Results and discussion

FTIR spectral analysis

The FTIR spectra NaY, PdY, NbPdY and TaPdY were shown in Fig. 1. The bands at 1640 and 3405 cm^{-1} indicate the surface silanol groups. The composites shows peak in the region of 1635 cm^{-1} was due to the in-plane bending vibrations of O-H. The NaY bands in range of 3560-3200 cm^{-1} are due to the surface hydroxyl groups and bands in region of 1140-450 cm^{-1} are due to the lattice Si-O-Si or Si-O-Al vibrations.[24] This excess of local positive charge in the zeolite framework with Nb or Ta was located by basic OH groups at 3610 and 3589 cm^{-1} for NbOH and TaOH group vibrations respectively.[25] The broadening of peak in the range of 3800-3400 cm^{-1} originate from the silanol groups of the NaY framework and metastable (Nb(Ta)=O-H$_2$O) and (Nb(Ta)-OH-H$_2$O) sites of the NbPdY and TaPdY.[26] The peak shift was observed from 1024 to 1008 cm^{-1} was due to formation of the Si-O-Nb(Ta) groups with (Si/Al)O$_4$ tetrahedron unites.
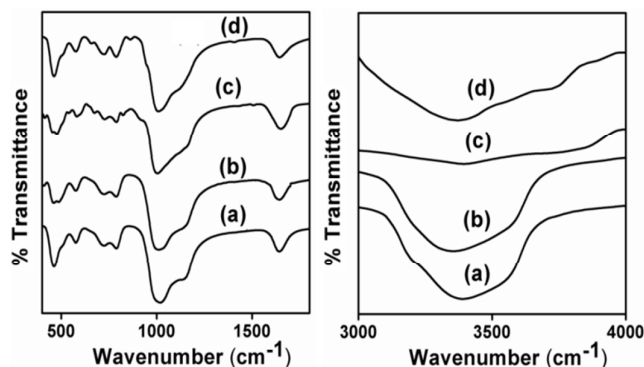
The peak shift in the regions at 3500 and 1024 cm^{-1} were only due to the presence of the transition metal in the cavity of the zeolite. It reveals no dealumination occurs during impregnation process.[27] Further, at lower frequency region of 935-920 cm^{-1} indicates the formation of dative or coordinative bond of both Nb-O and Ta-O with the (Si/Al)O$_4$ units. The low intensity bands appeared in the region of 485 cm^{-1} was due to Pd(II)-O bonding vibrations (Fig.1). The peaks at 660, 654 cm^{-1} indicates the presence of Nb-O and Ta-O frequencies respectively, but this was absent in the PdY.[28] This implies that the amount of Nb and Ta incorporated into the framework increases as the amount of Na$^+$ ions decreases. This observation suggesting that aluminosilicate frameworks were not changed during the impregnation. Hence, FTIR results may suggest the formation of monomeric forms of the Nb and Ta oxides in the zeolite cavities.[29] The FTIR spectral studies reveals that the stability of zeolite during the Nb(V) and Ta(V) impregnation process.

3.2 DRS UV-visible studies

The DRS UV-visible spectra NaY, PdY, NbPdY and TaPdY were provided in Fig. 2. The PdY, NbPdY and TaPdY shows the absorption bands at 406, 420, and 432 nm due to d-d transition, this peaks are absent in the NaY spectrum. NbPdY and TaPdY show bathochromic shift around 16 nm, when compared with that of PdY, it may be due to the formation Nb-O and Ta-O species in the cavity of the zeolite. The spectra of NbPdY and TaPdY exhibit a absorption band at 221 nm due to metal charge transfer transition and it may be the presence of mononuclear Ta(V) and Nb(V) in zeolite cavities. The absence of a band at higher wavelength (240-360nm) also suggesting the formation of monomeric Nb and Ta oxide species.[30,31] The less intensity peak in visible region indicates, it may be less percentage of the metal in zeolite cavities.
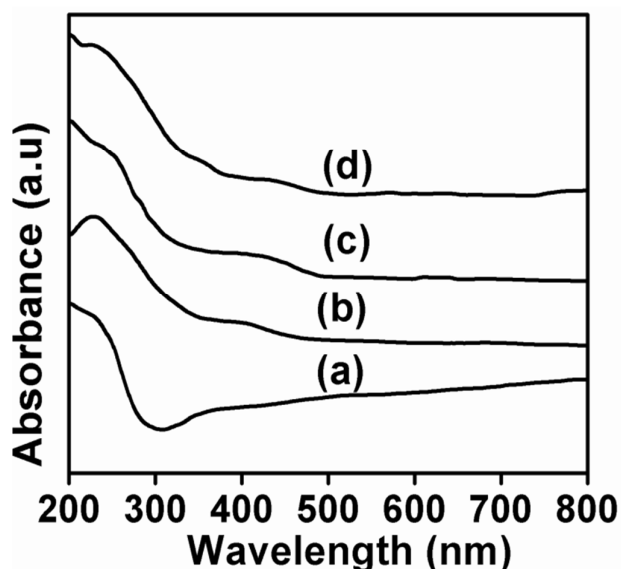

Fig. 1 FTIR spectra of the (a) NaY, (b) PdY, (c) NbPdY and (d) TaPdY

Fig. 2 DRS/UV-Visible spectra of the (a) NaY, (b) PdY, (c) NbPdY and (d) TaPdY

Powder XRD studies

The X-ray diffraction patterns of NaY, PdY, NbPdY and TaPdY crystalline nature was studied and given in the Fig. 3. All the materials shows diffraction patterns of (2 2 0), (3 1 1) and (3 3 1) peaks at 10°, 12° and 15.7° respectively.[32] The parent NaY has the peak diffraction peak intensity order $I_{331}>I_{220}>I_{311}$, but in case of the PdY, NbPdY and TaPdY slight decrease in peak intensities and negligible shift was observed when compared with NaY. This might be attributed to exchange of sodium ions by the di and penta valent metal ions. The parent NaY has peak intensity $I_{331}>I_{220}>I_{311}$, but in case of PdY, NbPdY and TaPdY the corresponding peak intensities $I_{331}>I_{311}>I_{220}$, $I_{331}>>I_{220}>I_{311}$ and $I_{331}>>I_{311}>I_{220}$ were observed.[32,33]
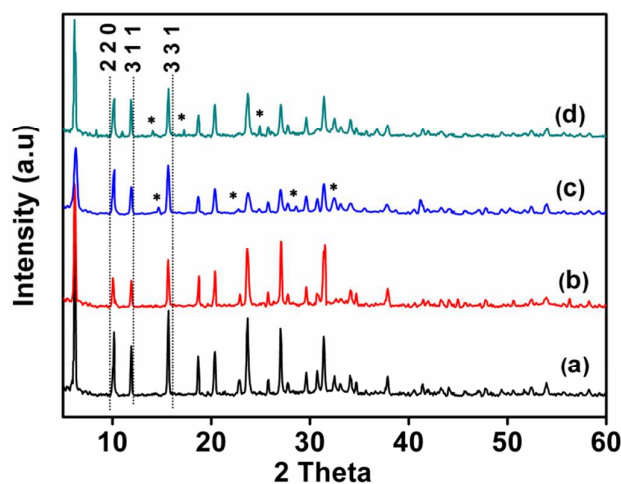

Fig. 3 The powder XRD patterns of (a) NaY, (b) PdY (c) NbPdY and (d) TaPdY

NbPdY shows new peaks at 14.56°, 22.76°, 28.85° and 33.95°. The TaPdY shows peaks at 10.98°, 14.07°, 17.44° and 36.18°, but these peaks were not seen in PdY and NaY. In case of PdY the decreaseing in peak intensity only observed when compared to that of NaY. This suggest that the allocation of Pd, Nb and Ta species in the cavities of the zeolite-Y. In another way during impregnation the guest metal make surface reduction of parent zeolite-Y. Hence, all the composites shows a slight change in a peak position, but all identical 2θ values suggest the crystalline nature of NaY does not change during impregnation process. The XRD pattern reveals the effective impregnation of the Nb and Ta oxide in the cavities of the NaY.

X-ray Photoelectron Spectroscopy analysis

XPS spectra of the NbPdY and TaPdY were shown in the Fig. 4. It reveals the presence of O, Na, Si, Al, Pd(II), Nb(V) and Ta(V). The XPS survey scan of all the composites shows a carbon signal (284.60 eV), which is always present in XPS spectra. The highly intense broad bands at 531.3 eV confirm the presence of oxygen atom. The C 1s, O 1s, Pd 3d, Nb 3d and Ta 4f appears at 284.1, 531.2, 334, 207 and 28 eV respectively.[34,35] Fig. 4(d) shows the Nb 3d core level spectra of the NbPdY and binding energy values at 208.3 eV and 205.8 eV for the Nb $3d_{3/2}$ and Nb $3d_{5/2}$ respectively, it

confirms Nb in +5 oxidation state. Fig. 4(e) shows the peaks at 230 and 242 eV related to Ta $4d_{5/2}$ and Ta $4d_{3/2}$ respectively for the TaPdY, where as Ta 4f spectra binding energy values observed at 26 eV and 29 eV for 4f7/2 and 4f5/2 eV respectively.[36,37] The XPS survey graph of the NaY was given in the Fig. S2.

The O 1s deconvoluted spectral trends suggests that more than one oxygen atoms are bonded with the Pd, Nb and Ta (Fig. S3†), hence can be fitted with multi peaks, which are characteristic of oxygen anions (O⁻) bound to the Nb and Ta with PdY. The lattice oxygen (530 eV) and oxygen in hydroxyl groups (531.3 eV)) further confirms the presence of hydroxyl groups. The parent NaY and Nb(Ta)PdY can exhibits different oxygen binding properties, when compared to that of NaY, Nb and Ta oxide forms with different valence states. The 4f spectrum of Ta in TaPdY also suggests the oxidation state of +5. Increase in the binding energy for oxygen atoms was due to the inter chelating tetrahedral silica group. The low intensity peaks of the composites were due to the presence of less metal percent in the cavities of the zeolite. The XPS analysis reveals the presence of Pd(II), Nb(V) and Ta(V) and coordinated oxygen with $(Si/Al)O_4$ moiety of the zeolite framework.

Nitrogen adsorption isotherms and BET analysis

The Brunauer-Emmett-Teller (BET), N_2 adsorption/desorption isotherms, surface area and the pore volume studies for the NaY, PdY, NbPdY and TaPdY were shown in the Fig. 5 (a-d). The pore size distribution curves of samples were evaluated from adsorption branches of the isotherms (inset diagrams) using the BJH method. These composites had type-IV isotherms. Initially a steep increment was observed upto p/p_0 of 0.3, this reflects their narrow pore size distribution, due to the capillary condensation of the pores. The surface area of zeolite was observed to be 600 m^2/g, but in case of PdY, NbPdY and TaPdY surface area were drastically reduced to 480 m^2/g, 440 m^2/g and 420 m^2/g respectively.[38] The average pore size of free zeolite was 2.2 nm and it was reduced to 1.8, 1.6 and 1.4 nm this may due to the presence of Pd, Nb and Ta species in the pores of zeolite. This confirms Nb and Ta oxides may have more reactive blockage sites in zeolite pores.

Thermal analysis

The TG/DTG curves of NaY, NbPdY and TaPdY in static air atmosphere were shown in Fig. S4(a-c)†. The residual mass are 86.8%, 82.89% and 82.02% for the NaY, NbPdY and TaPdY respectively. The DTG curve of NaY shows the single step decomposition upto 600 K with weight loss of 13.5%. Fig. S4(b&c)† shows the multistep thermal degradation NbPdY and TaPdY. From Fig. S4b† NbPdY show a first step a weight loss of 12.13% upto 577 K due to the loss of surface hydroxyl-hydrated ions. The second step weight loss of 2.66% observed upto 818 K and at 980 K a weight loss of 0.7% indicates the formation of metal oxide.[39] The TG/DTG patterns of the TaPdY show the weight loss of 12.32% at 500 K are due to hydrated molecules (Fig. S4c†). The further weight loss of 3.95% at 850 K corresponds to the removal of occluded ions. In final stage a mass loss of 1.2% upto 1150 K indicates that less percentage of the Nb and Ta in the composites. TGA analysis suggests the thermal stability of the composites, where the refractory metals were present of in the NaY matrix.
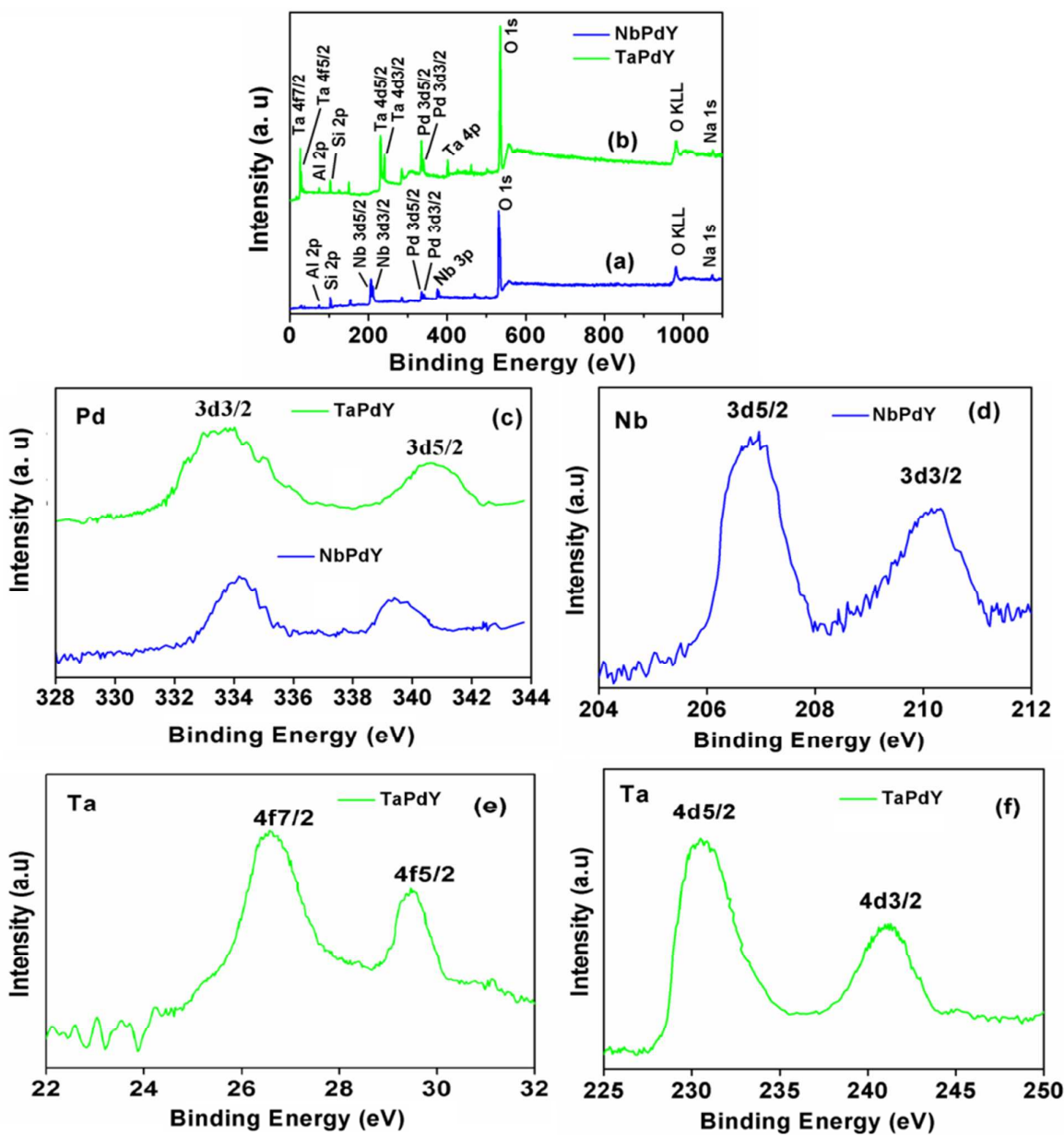
Fig. 4 XPS survey spectra of the (a) NbPdY and (b) TaPdY and their core level spectral traces of the (c) Pd(3d), (d) Nb(3d), (e) Ta(4f) and (f) Ta (4d)

FESEM analysis

Scanning electron micrographs of the NaY, PdY, NbPdY and TaPdY were shown in Fig. 6(a-d). It was inferred that NaY possess shape of the particle is cubic angular (Fig. 6a). Fig.6(b-d) SEM images of PdY, NbPdY and TaPdY shows a negligible change in the edges due to the impregnation of the Nb and Ta metals in the zeolite matrix. The crystal nature of PdY, NbPdY and TaPdY has not change even

after grafting the metals in zeolite.[40] From the Fig.6 the absence of surface particles suggesting the effective purification of the composites. The absence of the surface particles on the external zeolite surface also suggests the crystalline nature of zeolite during the purification process. From Fig. S5(a-d)† the EDX spectrum also suggesting the allocation of all elements, which were matched with XPS investigations.
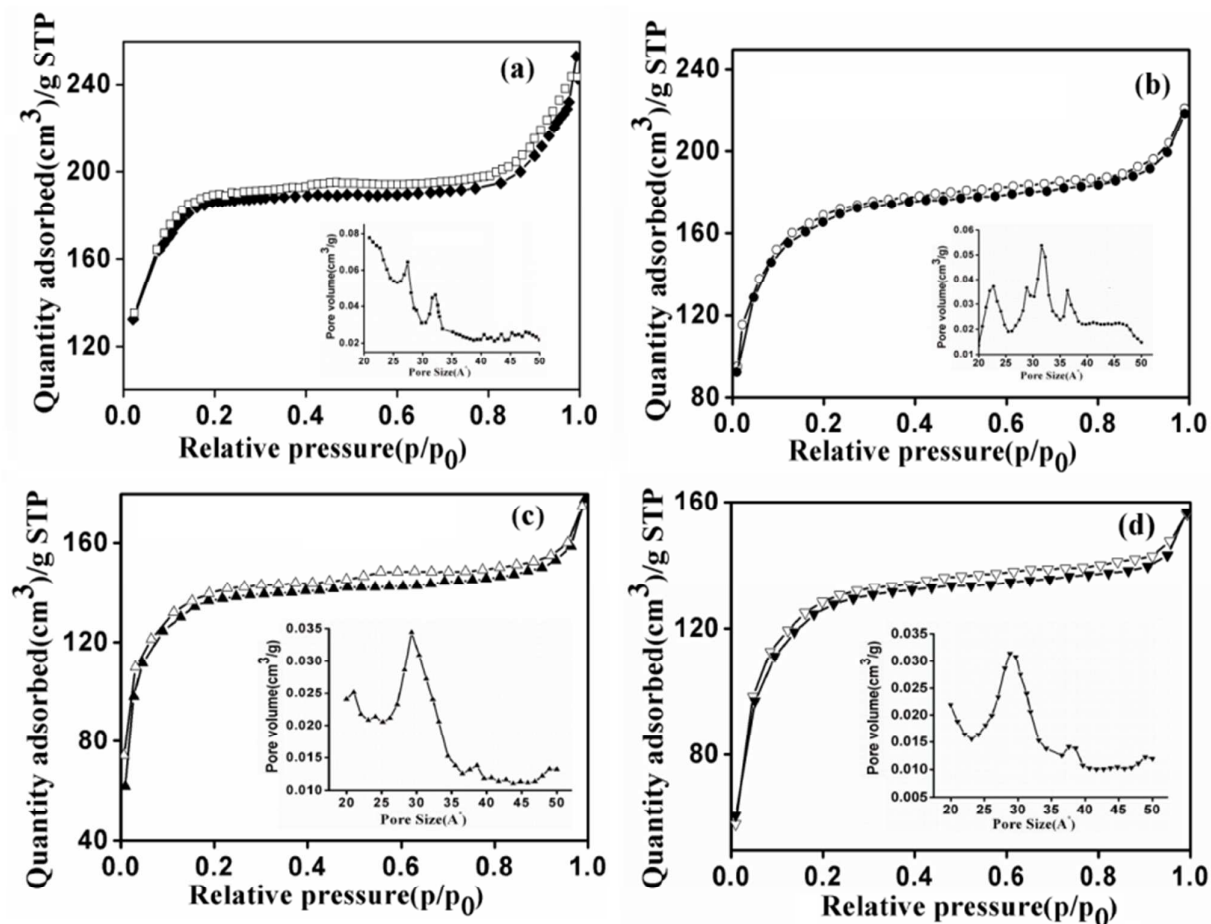
Fig. 5 The N_2 isotherms of the (a) NaY, (b) PdY, (c) NbPdY, (d) TaPdY and inset diagrams showing the pore size distribution curves

TEM analysis

Complementary to the SEM observations, TEM photography of NaY, NbPdY and TaPdY are shown in Fig. 7(a-c). This reveals that the structure of the NaY was rectangular spheroid (tablet shape) and its channels were well ordered. The NbPdY and TaPdY also shows spherical/angular shape, opaque nature and well ordered shape, but slight change in the surface edges and the negligible agglomeration was observed, when compared to parent zeolite.[40,41] The morphology of the NbPdY and TaPdY shows unique morphology of NaY even after encapsulation of the Nb and Ta oxide moiety in the NaY cavities.

Particle size studies

Particle size distribution curves of composites were obtained in the aqueous medium using the CILAS 1180 instrument. The particle size distribution curves obtained for the samples NaY, PdY, NbPdY and TaPdY in aqueous medium were provided in the Fig. S6(a-d)†. The particle size distribution curves of the parent NaY shows the mean diameter 6.9 μm, where as the PdY, NbPdY and TaPdY shows at 5.5, 3.3, 3.9 μm respectively. It indicates that, the impregnation of metal reduces the average mean diameter, it may be due to the

agglomeration of particle in the aqueous medium. This may be low loading efficiency of the Nb and Ta in the pore of the zeolite. The absence of bimodel histograms clearly suggests that no surface agglomerated Nb or Ta oxide particle. The better activity of NbPdY, TaPdY may be explained by active sites present in the zeolite cavities.[22]

Catalytic studies: Mechanistic issues for photochemical performance in the degradation of RhB and RR

Photocatalytic degradation of the RhB and RR in presence of NaY, PdY, NbPdY and TaPdY under visible light irradiation was studied. The percentage of degradation and kinetic parameter were calculated from the Lambert-Beers law ($A = \varepsilon.c.l$). The rate of reaction follows the first order rate equation given as bellow

$$\ln(\frac{Ct}{Co}) = -k\ app.t \qquad (2)$$

Here C_t is the concentration of the RhB and RR at different time, C_0 is the initial concentration, t is the time and k is the reaction rate constant in min^{-1}.
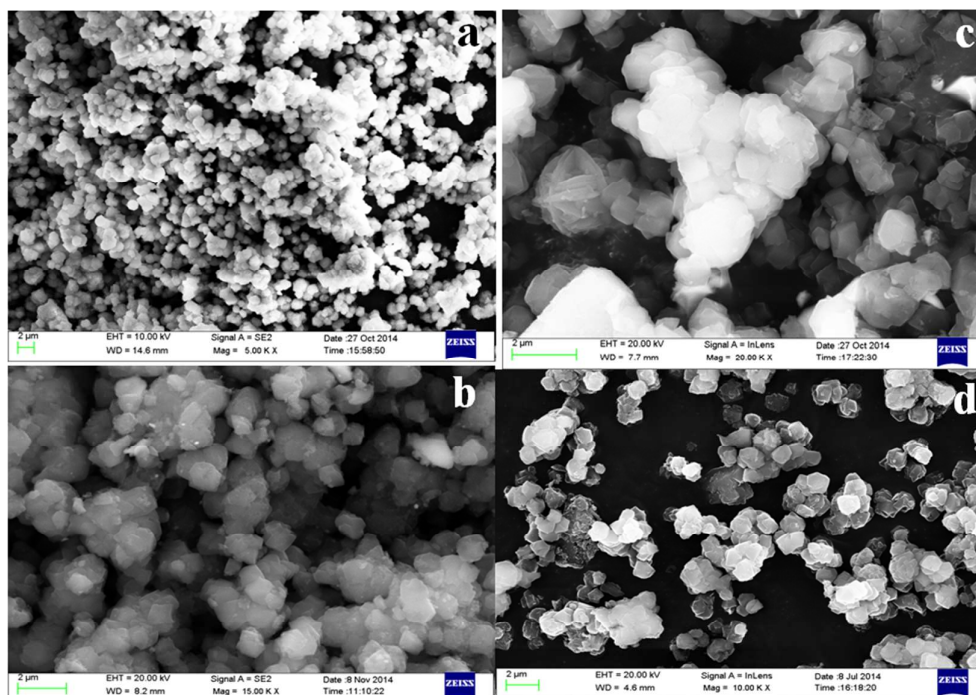
ARTICLE

Journal Name

Fig. 6 The SEM micrographs of the (a) NaY, (b) PdY, (c) NbPdY and (d) TaPdY
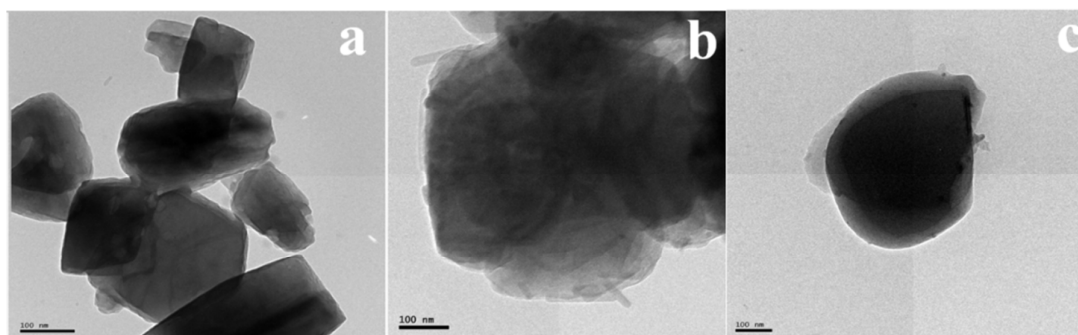

Fig. 7 TEM micrographs of the (a) NaY, (b) NbPdY and (c) TaPdY

The degradation efficiency was calculated by the optical absorption spectral analysis. The aliquot samples of reaction medium were collected and the consequence absorption changes were recorded at 554±1 nm and 519±1 nm for RhB and RR respectively.[42,43] The spectral changes were given in the Fig. S7&S8†. The NbPdY and TaPdY have more degradation performance, when compared to that of PdY and NaY. In case of the RhB degradation there is blue (hypsochromic) shift around 30 nm of absorption band for RhB dye aliquots, it suggests that the formation of de-ethylated RhB molecule. From Fig. 8(a&b) removal percentages of RhB are 10%, 64%, 91%, and 100%, where as in the case of RR 16%, 39%, 100% and 86% for the NaY, PdY, NbPdY and TaPdY respectively. The Nb and Ta metals can be enhance the acidity of zeolite during exchange process, The NbPdY and TaPdY could decrease the recombination of electron-hole pair and enhance

the photocatalytic performance. Particle size also impact on the activity of the photocatalysts, here the gradual decrease in the size also may lead to induced charge transfer in HOMO-LUMO energy levels and electron hole recombination has been prevented. The reaction was carried out at the fixed concentration of the all reactants. The catalytic reaction exhibits *pseudo*-first order kinetic parameters. Fig. 9(a&b) reveals the negative slope in both cases.[44] The rate constants of RhB were 0.0006 min^{-1}, 0.0067 min^{-1}, 0.0115 min^{-1} and 0.031 min^{-1} for NaY, PdY, NbPdY and TaPdY respectively. The rate constant of RR were 0.0004, 0.0017, 0.0113, 0.0054 min^{-1} for NaY, PdY, NbPdY and TaPdY respectively.

The NbPdY and TaPdY show higher activity, which enhances the photo generated electron pairs (e$^-$ and h$^+$). Photogenerated-holes and electrons may react with surface hydroxyl groups were adsorbed water or O_2 and then to generate the active oxidative ionic radical

ARTICLE　　**Journal Name**

($O_2^{\bullet-}$ and $^{\bullet}OH$) from reaction medium. The $O_2^{\bullet-}$ and $^{\bullet}OH$ radicals are very reactive and quickly oxidise organic species at the surface of the zeolite.[45] This acidity enhance the formation of active radical limits during the degradation time. During the metal reduction from M(II) to M(I)/M(0), the generation of the $^{\bullet}OH$ radical increase the catalytic activity. The generated peroxy radicals reacts with oxides of Nb, Ta leads to the formation of nascent oxygen.[46] this results the quick degradation of RhB and RR in reaction medium.　The pentavalent oxidation states of Nb and Ta provides the multiple electrons to vary the electrical conductivity. This was proposed for degradation of enlisted organics to carbon dioxide, water and other very less toxic minerals such as ammonia, nitrate and sulphates.[47]

Degradation of the 2CP and 4CP

The photocatalytic degradation of 2CP with NaY, PdY, NbPdY and TaPdY under visible light irradiation was studied. Degradation efficiency calculated by the optical absorption spectral analysis. The aliquot samples of reaction medium were collected and the consequence absorption changes were recorded at 220±1nm and 285(±1) for 4CP and 2CP respectively (Fig. S9&S10[†]).[48,49] At fixed amount of the catalysts and dye concentrations, the rate of the reaction follows the first order**.** Formation of $^{\bullet}OH$ radical has been substantiated by using mono chlorophenols. The NbPdY and TaPdY have more degradation performance, when compared to that of PdY and NaY. The removal percentages of 2CP are 3%, 54%, 97%, and 100%, whereas in the case of 4CP the removal percentages were 5%,

34%, 87%, and 100% for NaY, PdY, NbPdY and TaPdY respectively (Fig. 8c&d). The negative slope was observed for 2CP and 4CP oxidation reactions and shown in Fig. 9(c&d). In the case of 2CP, the rate constant values of 0.0001 min^{-1}, 0.0029 min^{-1}, 0.0083 min^{-1} and 0.0093 min^{-1} for NaY, PdY, NbPdY and TaPdY respectively. for the In the case of 4CP, the rate constant values of 0.0002, 0.0023, 0.0091 and 0.0295 min^{-1} for NaY, PdY, NbPdY and TaPdY respectively.

The 4CP has higher rate constant values when compared to 2CP, this is due to higher dissociation constant. The acid dissociation equilibrium for mono chlorophenol (Ph-OH) solution was Ph-OH → Ph-O[−]+H^{+}. Then formation of the HCl may leads to the acidic nature and its favourable for the generation of the OH ionic radicals available for the photo oxidation.[50,51] In liquid medium 4CP can easily enter in the cavities of the zeolite and it forms the active intermediates may cause the easy contact with active radicals and it reduce the degradation time. The photogenerated electron transfer to conduction band (e[−]) CB and further reacts with molecular oxygen leads the formation of hydroxy, perhydroxy radical ions, which are active in degrading organic pollutants.[52-55] The proposed radical-ions mechanism for RhB, RR, 2CP and 4CP degradation was illustrating in the Fig. 10. The experiment in dark degradation efficiency is near to low because of the poor ability to donate electrons to surface active catalyst. It could conclude that there was no interaction between halo phenols and catalysts.
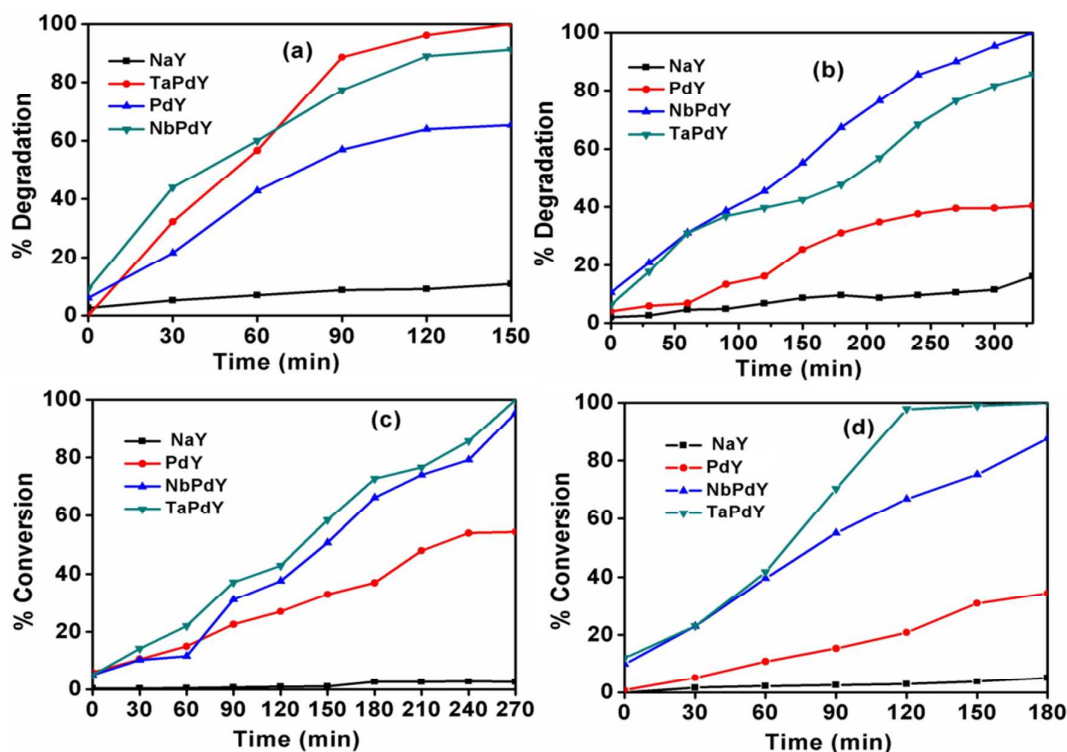

Fig. 8 The graph of time Vs % conversion in the degradation of (a) RhB, (b)RR, (c) 2CP and (d) 4CP for the NaY, PdY, NbPdY and TaPdY respectively
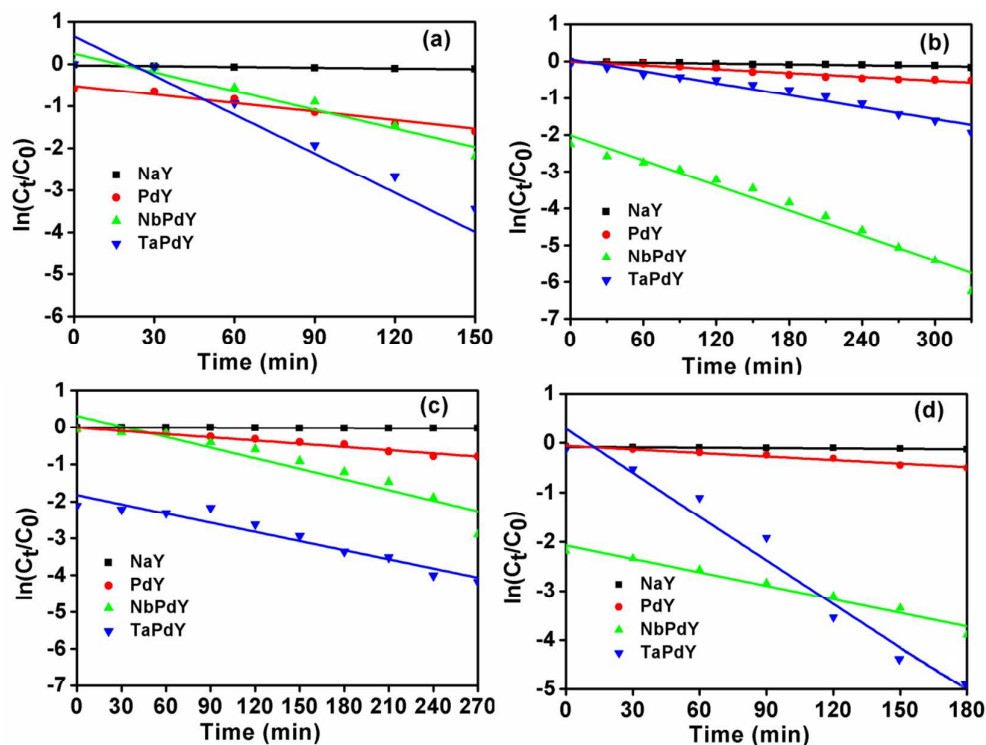
Fig. 9 Kinetic plots of time Vs % $\ln(C_t/C_0)$ in the degradation of (a) RhB, (b) RR, (c) 2CP and (d) 4CP for the NaY, PdY, NbPdY and TaPdY respectively
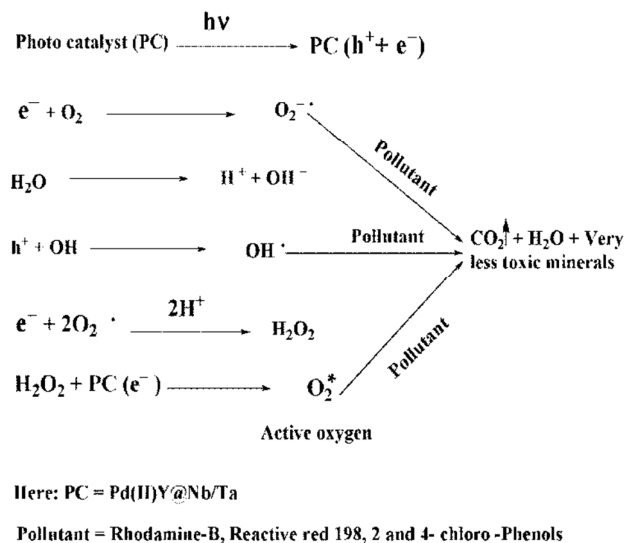

Here: PC = Pd(II)Y@Nb/Ta

Pollutant = Rhodamine-B, Reactive red 198, 2 and 4- chloro -Phenols

Fig. 10 The proposed radical-ions mechanism for RhB, RR, 2CP and 4CP degradation.

The reused photocatalytic studies of PdY, NbPdY and TaPdY and overall percentage of the degradation were provided in the Fig.11. After recycle of the composites from the reaction medium by nano-filteration and dried at 373 K under vacuum for 4 h. The recovered catalyst stability was confirmed by the powder XRD and DRS/UV-visible it show the similar diffraction peaks and electronic transition respectively (Fig. S11&S12)†.After recycle of the composites from the reaction medium by nano-filteration and dried at 373 K under vacuum for 4 h. The recovered catalyst stability was confirmed by the powder XRD and DRS/UV-visible it show the similar diffraction peaks and electronic transition respectively (Fig. S11&S12)†. The SEM image of the NbPdY and TaPdY also shows unique morphology with that of fresh catalyst (Fig. S13)†. The activity was checked in five cycles towards the RhB, RR, 2CP and 4CP and compared those of fresh catalyst. The recycling catalyst also has shown comparable activity with fresh catalyst. All the spectrophotometric measurements at initial and final time noted for reused photocatalysts. The overall percentage conversion also calculated by equation (1). The Fig. 11 shows plot of number of cycle and overall degradation percentage in the all catalytic reactions.

Conclusions

The NaY impregnated with Nb, Ta and Pd composites were synthesised. The composites impregnation and stability were studied by several spectroscopic, sorption, thermal analysis, and microscopic techniques. These methods confirmed the presence of Nb and Ta in the monomeric, pentavalent form in zeolite cavity. FTIR spectra reveals the presence of the Nb and Ta oxides with $(Si/Al)O_4$ moiety
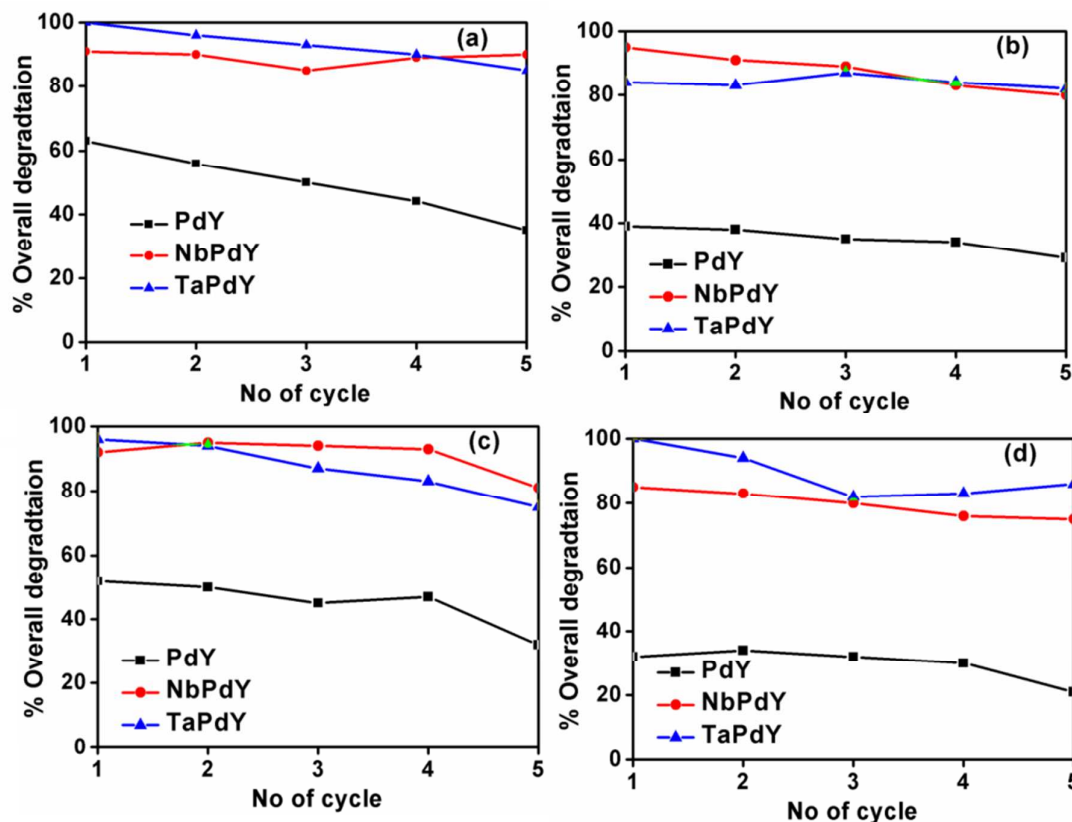
Fig. 11 The plots of No. of Cycle Vs overall percentage of conversion for the (a) RhB, (b) RR, (c) 2CP and (d) 4CP dye in presence of PdY, NbPdY and TaPdY

of the zeolite. XPS analysis suggested that the presence of all elements in the zeolite cavities. XRD and surface area measurements reveals the decreases in surface area values due to surface reduction during doping of Nb and Ta oxides of Pd exchanged zeolite. The microscopic analysis and EDX spectral traces indicate absence of Nb and Ta traces on the surface of the zeolite. The entire composite used as photocatlysts in the degradation of RhB, RR, 2CP and 4CP. The NbPdY and TaPdY composites show higher photocatalytic efficiency than NaY and PdY. Percentage of degradation and rate of reaction was more for the NbPdY and TaPdY. The degradation of the dyes follows the *pseudo*-first order kinetics. The recovery and reused catalysts also shown comparable activity with the fresh catalysts.

Acknowledgements

References

[1] F. Chen, F. Yan, Q. Chen, Y. Wang, L. Han, Z. Chen and S. Fang, *Dalton Trans*. 2014, **43,** 13537.

[2] K. C. Gupta and A. K. Sutar, *Coord. Chem. Rev*. 2008, **252**, 1420.

[3] P. Ciesla, P. Kocot, P. Mytych and Z. Stasicka, *J. Mol. Catal. A*: *Chem*. 2004, **224**, 17.

[4] D. Gompel, M. N. Tahir, M. Panthofer, E. Mugnaioli, R. Brandscheid, U. Kolb and W. Tremel, J. *Mater. Chem. A,* 2014, **2,** 8033.

[5] Y.J. Acosta-Silva, R. Nava, V. H. Morales, S. A. M. Sanchez, M. L. Gerrera and B. Pawelec, *Appl. Catal., B: Environ* 2011, **110**, 108

[6] I. Nowak and M. Ziolek, *Chem. Rev.* 1999, **99,** 3603.

[7] C. M. A. Parlett, K. Wilson and A. F. Lee, *Chem. Soc. Rev.* 2013, **42,** 3876.

[8] F. Hoffmann, M. Cornelius, J. Morell, and M. Frb, *Angew. Chem. Int. Ed.* 2006, **45,** 3216.

[9] D. K. Mishra, A. A. Dabbawala and J. S. Hwang, *J. Mol. Catal. A: Chem.* 2013, **76**, 63.

[10] A. Modak, A. K. Barui, C. R. Patra, and A. Bhaumik, *Chem. Commun.* 2013, **49, 7**644.

[11] FAO/WHO Expert Meeting on the Application of Nanotechnologies in the Food and Agriculture Sectors: Potential Food Safety Implications, 2009, http://www.who.int/foodsafety/fs_management/meetings/nanoj une09/en/index .html 3/9/2010.

[12] C. Tiozzo, C. Bisio, F. Carniato and M. Guidotti, *Catal. Today.* 2014, **235,** 49.

[13] X. Shen, L. Zhu, N. Wang, L. Yec and H. Tang, *Chem. Commun.* 2012, **48, 7**88.

[14] G. R. Ramanjaneya and S. Balasubramanian, *RSC Adv,* 2015, **5:** 53979.

[15] A. Boisen, I. Schmidt, A. Carlsson, S. Dahl, M. Brorson and C. J. H. Jacobsen, *Chem. Commun.* 2003, 958.

[16] M. T. Weller, J. Chem. Soc. *Dalton Trans.* 2000, 4227.

[17] J. Dasgupta, J. Sikder, S. Chakraborty, S. Curcio and E. Drioli, *Biochem. Eng. J.* 2015, **93,** 17.

[18] M. Czaplicka, *J. Hazard. Mater.* 2006,**134**, 45.

[19] R. H. Milller, S. Jorks, S. Kleinsteuber and W. Babel, *Microbiol. Res.* 1999, **154**, 241.

[20] R. Alimoradzadeh, A. Assadi, S. Nasseri and M. R. Mehrasbi, *Iran. J..Environ. Health Sci & Eng.* 2012, **9,** 1.

[21] Y. Zhanga, Z. Tanga, X. Fua and Y. J. Xua, *Appl. Catal., B: Environ.* 2011, 106, 445.

[22] A. C. Pradhan, K. M. Parida and B. Nanda, *Dalton Trans.* 2011, **40,** 7348.

[23] V. F. Surganov, A. M. Mozalev and V. A. Lastochkina, *J. Appl Spectrosc, 2*000, **67,** 412.

[24] J. M. Jehng, W. C. Tung, C. H. Huang, and I. E. Wachs, *Microporous Mesoporous Mater.* 2007, **99**, 299.

[25] A. Corma, F. X. L. Xamena, C. Prestipino, M. Renz, and S. Valencia, *J. Phys. Chem. C.* 2009, **133,** 11306.

[26] A. M. Prakash and L. Kevan, *J. Am. Chem. Soc.* 1998, **120,** 13148.

[27] F. Tielens and S. Dzwiga, *J. Chem. Phys. Lett.* 2010, **501,** 59.

[28] A. Wojtaszek, M. Ziolek and F. Tielens, *J. Phys. Chem. C.* 2012, **116,** 2462.

[29] F. Tielens, *J. Mol. Struct.: THEOCHEM.* 2009, **903,** 23–27.

[30] S. Dzwigaj, Y. Millot, C. Methivier and M. Che, *Microporous Mesoporous Mater.* 2010, **130**, 162.

[31] S. Dzwigaj, Y. Millot and M. Che, *Catal Lett,* 2010, **135,** 169.

[32] M. R. Maurya, S. J. J. Titinchi and S. Chand, *J. Mole Catal A: Chem.* 2004, **214,** 257.

[33] J. H. Kwak, D. Tran, S. D. Burton, J. Szanyi, J. H. Lee and C. H. F. Peden, *J. Catal.* 2012, **287,** 203.

[34] G. R. Ramanjaneya and K. Chennakesavulu, *J. Mol. Struct.* 2014, **1075,** 406.

[35] M. Chandrasekhar, S. V. J. Chandra and S. Uthanna, *Indian J. Pure Appl. Phy.* 2009, **47,** 49.

[36] C. D. Wagner, W. M. Riggs, L. E. Davis and G. E. Muilnberg, Hand book of X-ray Photoelectron spectroscopy, Perkin-Elmer, Minnesota, 1979.

[37] J. Wu, J. Wang, H. Li, Y. Du, X. Jia and B. Liu, *Cryst. Eng. Comm.* 2014, **16,** 9675.

[38] D. M. Antonelli and J. Y. Ying, *Chem. Mater.* 1996, **8,** 874.

[39] R. Uddin, Q. Xuanhui, L. Ping, L. Zhang, M. Ahmad, M. Z. Iqbal, M. Y. Rafique and M. H. Farooq, *RSC Adv.* 2012, **2,** 4891.

[40] Y. Lin, H. Lin, H. Wang, Y. Suo, B. Li, C. Kong and L. Chen, *J. Mater. Chem. A,* 2014, **2,** 14658.

[41] G. R. Ramanjaneya, S. Balasubramanian and K. Chennakesavulu, *J. Mater. Chem. A,* 2014, **2,** 15598.

[42] Q. Wang, C. Chen, D. Zhao, W. Ma and J. Zhao, *Langmuir.* 2008, **24,** 7338.

[43] G. Moussavi and R. Khosravi, *Bioresour. Technol.* 2012, **119,** 66.

[44] Z. Xiong, L. L. Zhang and X. S. Zhao, *Chem. Eur. J.* 2011, **17,** 2428.

[45] M. Ziolek, I. Sobczak, P. Decyk and l. Wolski, *Catal. commun.* 2013, **37,** 85.

[46] J. F. Guo, B. Ma, A. Yin, K. Fan and W. L. Dai, *Appl. Catal. B: Environ.* 2011, **101,** 580.

[47] G. Li, Y. Zhang, L. Wu, F. Wu, R. Wang, D. Zhang, J. Zhu and H. Li, *RSC Adv.* 2012, **2,** 4822.

[48] M. Uchida and A. Okuwaki, *J. Solution Chem*. 2003, **2,** 19.

[49] M. Y. Guo, A. M. C. Ng, F. Liua, A. B. Djurisic and W. K. Chan. *Appl. Catal. B: Environ,* 2011, **107,** 150.

[50] P. C. Sla, P. Kocot, P. Mytych and Z. Stasicka, *J. Mol. Catal. A: Chem.* 2004, **224,** 7.

[51] M. Gmurek, J. Mosinger and J. S. Miller, *Photochem. Photobiol. Sci.* 2012, **11,** 1422.

[52] L. Zhao, T. Cui, Y. Li, B. Wang, J. Han, L. Han and Z. Liu , *RSC Adv.,* 2015, **5,** 64495.

[53] K. Chennakesavulu and G. R. Ramanjaneya, *RSC Adv.* 2015, 5, 56391.

[54] L. H. Wee, N. Janssens, J. Vercammen, L. Tamaraschi, L. C. J. Thomassen and J. A. Martens *J. Mater. Chem. A,* 2015, **3,** 2258.

[55] S. Martha, P. C. Sahoo and K. M. Parida, *RSC Adv.,* 2015, **5,** 61535.

RSC Advances Accepted Manuscript

Graphical abstract

Zeolite encapsulated active metal composites and their photocatalytic studies for the rhodamine-b, reactive red-198 and chloro- phenols

G. Ramanjaneya Reddy[a], S. Balasubramanian[a], K. Chennakesavulu[b,c*]